International Journal of Computational Intelligence in Control, 7(2), 2015

SYNCHRONIZATION OF COUPLED NEURONS USING A TSK-TYPE RECURRENT FUZZY NEURAL NETWORK WITH ASYMMETRIC GAUSSIAN MEMBERSHIP FUNCTIONS

Chun-Fei Hsu

Department of Electrical Engineering, Tamkang University, No. 151, Yingzhuan Rd.
Danshui Dist., New Taipei City 25137, Taiwan (R.O.C.)

ABSTRACT: In this paper, a Takagi-Sugeno-Kang (TSK)-type recurrent fuzzy neural network (TRFNN) with asymmetric Gaussian membership functions is studied. The asymmetric Gaussian membership function is constituted by a center, a left-sided spread and a right-sided spread. Since the weight of output layer uses a functional-type form in TRFNN, the TRFNN provides a powerful representation. In addition, this paper proposes an adaptive TSK-type recurrent fuzzy neural control (ATRFNC) system for the synchronization of coupled neurons. The proposed ATRFNC system is composed of a neural controller and a robust compensator. The neural controller uses a TRFNN to online mimic an ideal controller and the robust compensator is designed to dispel the approximation error between the ideal controller and neural controller. All the controller parameters of the proposed ATRFNC system are tuned in the sense of Lyapunov theorem, thus the stability of the closed-loop system can be guaranteed. Moreover, a proportional-integral type learning algorithm is derived to speed up the convergence of the tracking error. Finally, some simulation results verify that the proposed ATRFNC system can achieve a favorable synchronization performance without occurring chattering phenomena.

Keywords: Recurrent neural network, adaptive control, neural control, coupled nonlinear chaotic system, synchronization.

I. INTRODUCTION

Taking the advantage of neural networks in learning from processes, this is an active research topic in the area of fuzzy neural networks (FNNs) (Juang and Lo, 2008; Lin and Lee, 1996; Nauck *et al.*, 1997). For a controller design, since parameterized FNNs can approximate an unknown system dynamics or an ideal controller, the FNN-based adaptive neural control approaches have grown rapidly in many previous published papers (Chen *et al.*, 2008; Chen and Chen, 2009; Hsu, 2007; Lin, 2008; Miguel and Yu, 2009). It is important that the basic issue of the FNN-based adaptive neural controllers is to provide online learning algorithms that do not require preliminary off-line training. Generally, FNNs can be divided into two types, which are Mamdani-type FNN and Takagi-Sugeno-Kang (TSK)-type FNN. The output weights are equipped with a singleton-type form in a Mamdani-type FNN but with a functional-type form in a TSK-type FNN. Thus, a TSK-type FNN provides more powerful representation than a Mamdani-type FNN (Wai and Chen, 2004). As known, the existing TSK-type FNNs are classified as feedforward neural networks which are static mapping. Without the aid of tapped delays, they are unable to represent a dynamic mapping. To deal with dynamic problems, a TSK-type recurrent FNN (TRFNN) is developed to capture the dynamical response (Chen, 2010; Juang, 2002).

Since the number of neurons in TRFNN is finite for real-time practical applications, the approximation errors cannot be evitable. To ensure the stability of the TRFNN-based adaptive neural control systems, a switching compensator should be designed. The most used switching

Corresponding author: E-mail: fei@ee.tku.edu.tw

compensator is liked as a sliding-mode control which requires the bound of the approximation error. However, the switching compensator causes the chattering phenomena in the control effort to wear the bearing mechanism (Lin and Hsu, 2003). To confront this problem, a continuous saturation function with a boundary layer thickness was used to replace the switching sign function (Lin and Hsu, 2003). However, there is a trade-off problem between chattering phenomena and control accuracy arises.

To reduce the chattering phenomena, some researchers combined the robust control approach to attenuate the influence of the approximation error (Tseng, 2008; Yang and Zhou, 2005). The better tracking performance can be achieved as specified attenuation level is chosen smaller; however, the control effort may lead to a large control signal. Shahnazi and Akbarzadeh-T (2008) proposed a proportional-integral structure compensator which does not require the bound of the approximation error. The proportional-integral structure compensator made the computation loading heavy so it is not suitable for the online practical applications. A supervisory compensator combining the sliding-mode control and the adaptive control by using a modulation function is proposed to deal with the approximation error (Chen and Chen, 2009). However, the proposed approximation error bound estimation law will make the estimation error bound go to infinity.

Chaotic system is a nonlinear deterministic system that displays complex, noisy-like and unpredictable behavior, so how to synchronize chaotic system become a great deal in engineering community (Chen, 2002; Chen *et al.*, 2010; Lin *et al.*, 2010). Generally, there are two ways to synchronize the system from the synchronization point of view. The first one is self-synchronization which is related with natural coupling. The second one is related with artificial coupling which uses a controller as the feedback between neurons (Wang *et al.*, 2004). For the natural coupling without control, identical coupled neurons can eventually synchronize only when the coupling strength is above certain critical value which may be beyond the physiological condition. Therefore, artificial coupling is of much significance and necessity to synchronize the neuronal system (Wang *et al.*, 2004; Wang *et al.*, 2006; Zhang *et al.*, 2007).

In this paper, the synchronization control of two coupled chaotic FitzHugh-Nagumo neurons under electrical stimulation is investigated. If the exact model of the two coupled neurons is known, there exists an ideal controller to achieve a favorable control performance by possible canceling all the system dynamics (Slotine and Li, 1991). A tradeoff between the stability and accuracy is necessary for the performance of ideal controller. To attack this problem, an adaptive TSK-type recurrent fuzzy neural control (ATRFNC) system with a proportional-integral (PI)-type learning algorithm is proposed. The proposed ATRFNC system is composed of a neural controller and a robust compensator. All the parameters of the proposed ATRFNC system are tuned in the sense of Lyapunov theorem, thus the stability of the closed-loop system can be guaranteed. Finally, some simulation results validate that the favorable synchronization performance can be achieved by using the proposed ATRFNC system.

II. TWO NEURONS COUPLED WITH A GAP JUNCTION

In neural systems, a gap junction is an electrical synapse that is a mechanical and electrically conductive link between two adjacent neurons. Through gap junctions, neurons can communicate with each other, and the synaptic current is proportional to the difference of membrane potentials between a neuron and its neighbors. This paper considers a model of the two coupled chaotic FitzHugh-Nagumo neurons with a gap junction as shown in Fig. 1 which can be described as (Wang *et al.*, 2004).

Master system:

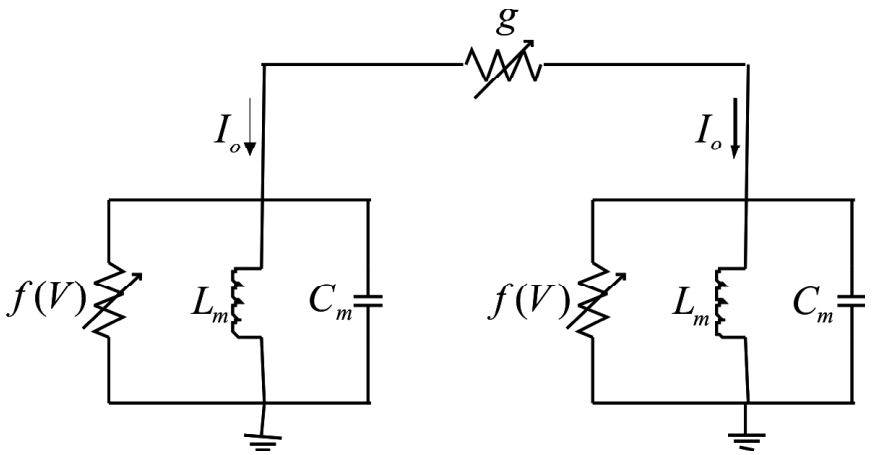

Figure 1: The Circuit Diagram of Two Coupled Neurons

$$\begin{aligned}\dot{X}_1 &= X_1(X_1-1)(1-rX_1) - Y_1 - g(X_1 - X_2) + I \\ \dot{Y}_1 &= bX_1\end{aligned} \tag{1}$$

Slave system:

$$\begin{aligned}\dot{X}_2 &= X_2(X_2-1)(1-rX_2) - Y_2 - g(X_2 - X_1) + u + I \\ \dot{Y}_2 &= bX_2\end{aligned} \tag{2}$$

where X_i and $Y_i (i = 1,2)$ are rescaled membrane voltage and recovery variable of two neurons, respectively, g is the coupling strength of gap junction, $I = \frac{A}{\omega}\cos\omega t$ is the external electrical stimulation with A and $\omega = 2\pi f$ are the amplitude and frequency, respectively, and u is the control effort. The parameters of the two neurons coupled chaotic systems are selected as A = 0.1, b = 1, r = 10 and f = 0.1271. For observing the chaotic unpredictable behavior, the open-loop system behavior with u = 0 was simulated with a initial condition (X_1, X_2, Y_1, Y_2) = (1, 0, 1, 0). To synchronize the two coupled chaotic FitzHugh-Nagumo neurons, define tracking errors $e_1 = X_1 - X_2$ and $e_2 = Y_1 - Y_2$. The time responses of the uncontrolled coupled neurons for g = 0.01 and g = 1.0 are shown in Figs. 2 and 3, respectively. The phase portraits on plan of $X_1 - Y_1$ are shown in Figs. 2(a) and 3(a), the phase portraits on plan of $X_2 - Y_2$ are shown in Figs. 2(b) and 3(b), the phase portraits on plan of $X_1 - X_2$ are shown in Figs. 2(c) and 3(c), the phase portraits on plan of $Y_1 - Y_2$ are shown in Figs. 2(d) and 3(d), the time responses of error e_1 are shown in Figs. 2(e) and 3(e), and the time responses of error e_2 are shown in Figs. 2(f) and 3(f). According to the simulation results, the synchronization occurs only when the coupling strength of gap junction satisfies some condition.

The chaos synchronization problem has the following features: the trajectories of a slave system can track the trajectories of a master system, thus an error dynamical system can be expressed as

$$\begin{aligned}\dot{e}_1 &= X_1(X_1-1)(1-rX_1) - X_2(X_2-1)(1-rX_2) - 2ge_1 - e_2 - u \\ \dot{e}_2 &= be_1\end{aligned} \tag{3}$$

Then, the error dynamic can be rewritten in a vector form as

$$\dot{\mathbf{e}} = \mathbf{A}\mathbf{e} + \mathbf{b}[z(\mathbf{x}) - u] \tag{4}$$

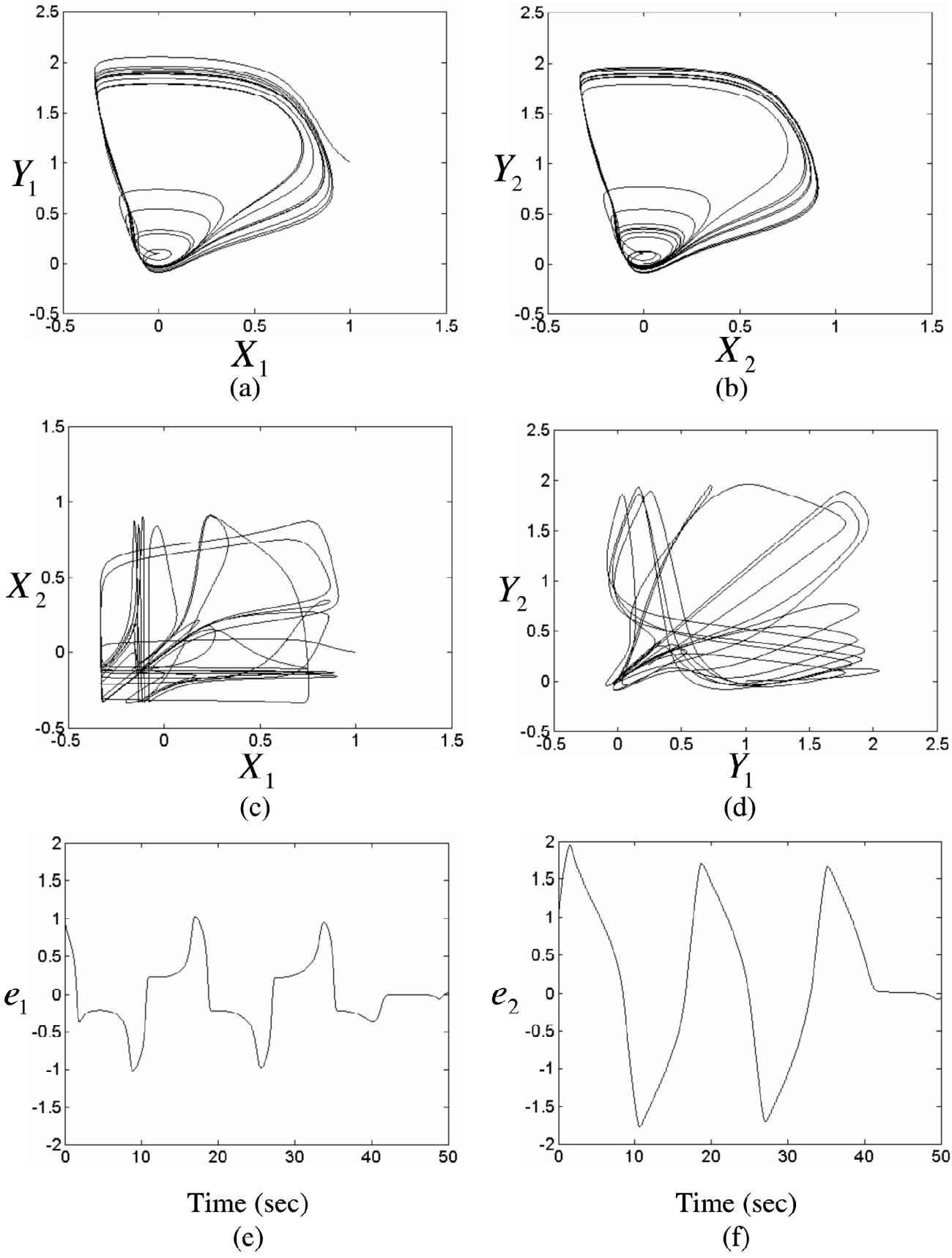

Figure 2: The Portraits on Different Planes without Control for $g = 0.01$

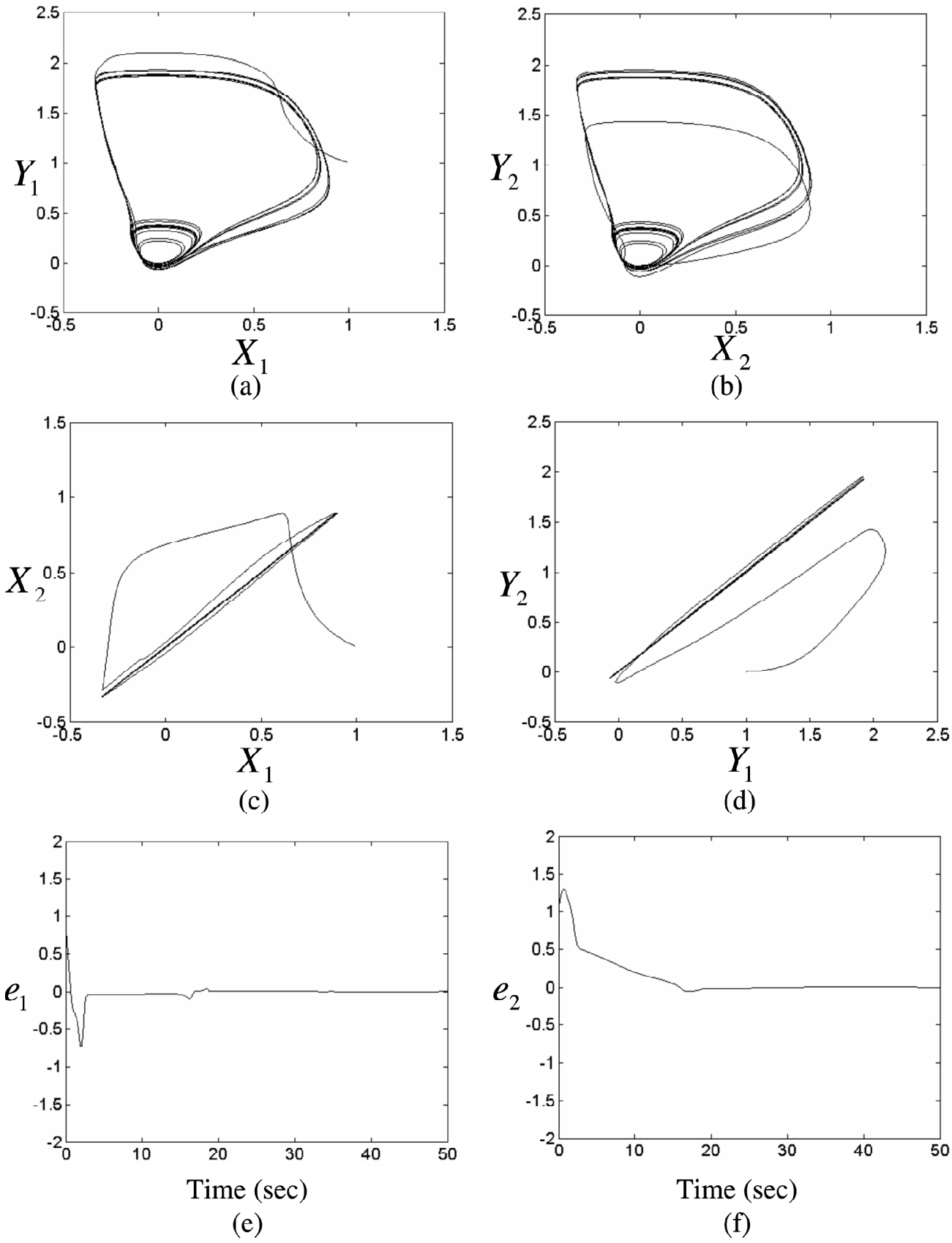

Figure 3: The Portraits on Different Planes without Control for $g = 1.0$

where $\mathbf{x} = [X_1, X_2]^T$ is the state vector, $\mathbf{e} = [e_2, e_1]^T$ is the state error vector, $\mathbf{A} = \begin{bmatrix} 0 & b \\ -1 & -2g \end{bmatrix}$, $\mathbf{b} = [0,1]^T$, and $z(x) = X_1(X_1 - 1)(1 - rX_1) - X_2(X_2 - 1)(1 - rX_2)$ is the system dynamics. Assume all the parameters in (4) are known, there exists an ideal controller as (Slotine and Li, 1991)

$$u^* = z(\mathbf{x}) + \mathbf{ke} \tag{5}$$

where $\mathbf{k} = [k_1, k_2]$ is the feedback gain vector. Substituting (5) into (4), the error dynamic becomes to

$$\dot{\mathbf{e}} = (\mathbf{A} - \mathbf{bk})\mathbf{e} = \Lambda\mathbf{e} \tag{6}$$

where $\Lambda = \mathbf{A} - \mathbf{bk}$. Suppose the feedback gain vector $\mathbf{k}$ is chosen to correspond with the coefficients of a Hurwitz polynomial, it implies that $\lim_{t\to\infty} e = 0$ for any starting initial conditions. Since the system dynamics $z(\mathbf{x})$ may be unknown or perturbed, the ideal controller (5) cannot be precisely obtained.

III.ATRFNC SYSTEM DESIGN

To solve this problem of system dynamics determination, this paper proposes an ATRFNC system as shown in Fig. 4 which is composed of a neural controller and a robust compensator, i.e.

$$u_{arfn} = \hat{u}_{nc} + u_{rc}\,. \tag{7}$$

The neural controller $\hat{u}_{nc}$ utilizes a TRFNN to mimic the ideal controller in (5) and the robust compensator u_{rc} is used to compensate for the difference introduced by the neural controller.

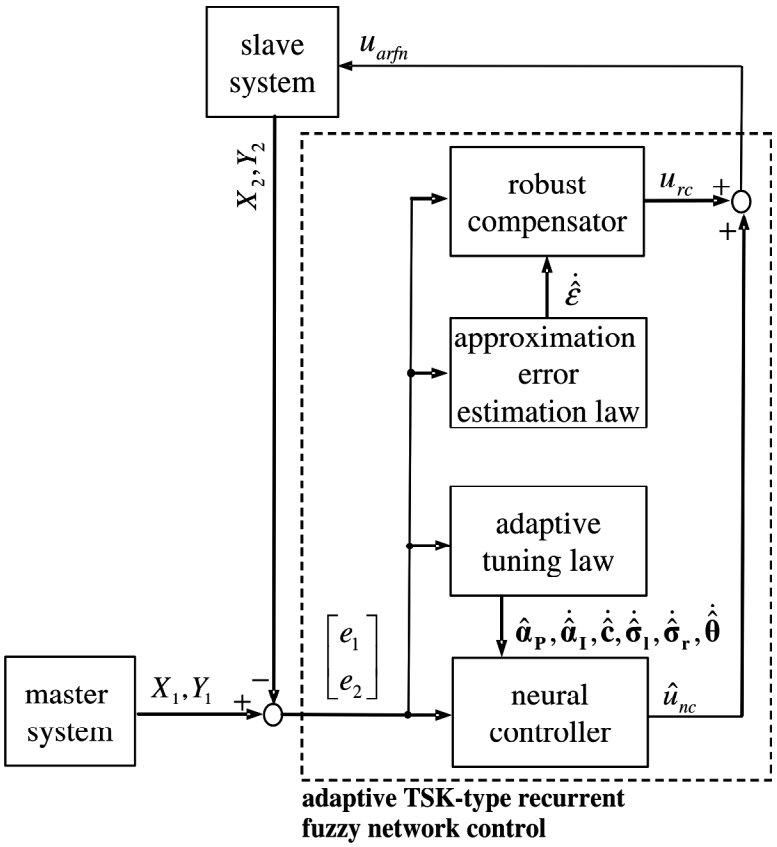

Figure 4: Block Diagram of the ATRFNC for the Two Neurons Coupled Chaotic Systems

(A) TRFNN

The configuration of TRFNN as shown in Fig. 5 is composed of the input, the membership, the rule, the TSK and the output layers (Cheng *et al.*, 2007). The recurrent feedback is embedded in the network by adding feedback connections in the membership layer. The used asymmetric Gaussian membership function is constituted by a center, a left-side variance, and a right-side variance. The signal propagation and the basic function in each layer are as follows:

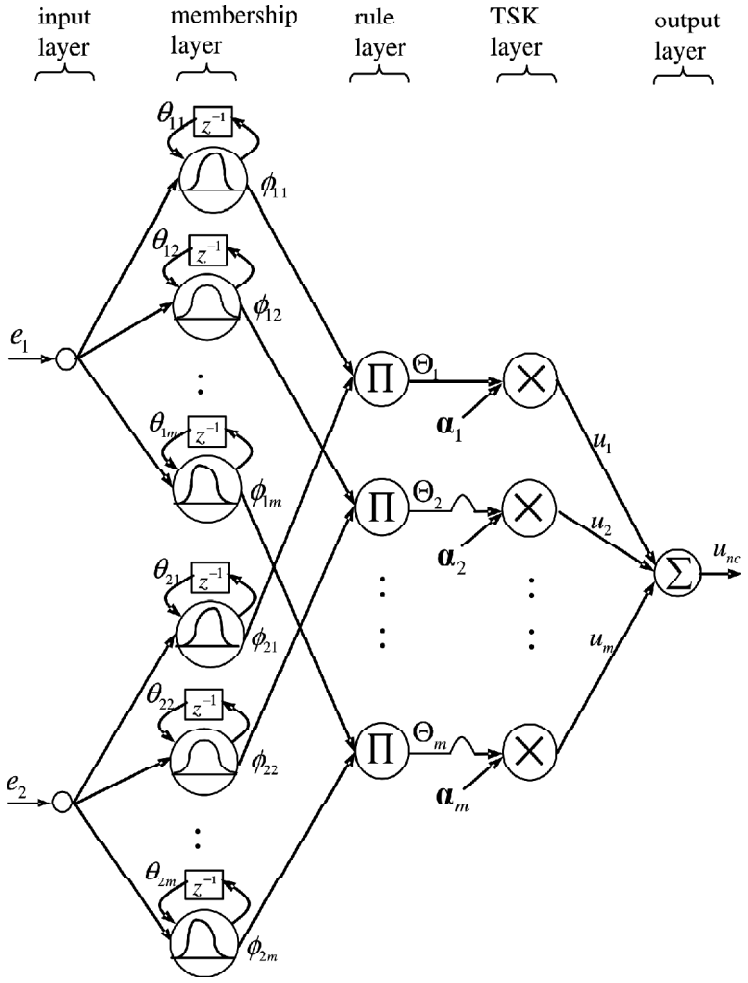

Figure 5: TRFNN with Asymmetric Gaussian Membership Functions

Layer 1 - Input layer: No function is performed in this layer. The node only transmits input values to layer 2.

Layer 2 - Membership layer: In this layer, each node performs a membership function and acts as a unit of memory. The asymmetric Gaussian function is adopted as the membership function. For the *j*th node (Cheng *et al.*, 2007; Velayutham and Kumar, 2005)

$$\phi_{ij} = \begin{cases} \exp[-\dfrac{\left(e_i + \phi_{ij}^{p}\theta_{ij} - c_{ij}\right)^2}{\left(\sigma_{ij}^{l}\right)^2}], \ if \ \ -\infty < x_i \le c_{ij} \\ \qquad\qquad\qquad\qquad\qquad\qquad\qquad\qquad , j = 1,2,...,m \\ \exp[-\dfrac{\left(e_i + \phi_{ij}^{p}\theta_{ij} - c_{ij}\right)^2}{\left(\sigma_{ij}^{r}\right)^2}], \ if \ \ c_{ij} \le x_i < \infty \end{cases} \tag{8}$$

where c_{ij} is the mean, σ_{ij}^{l}, σ_{ij}^{r} and θ_{ij} are the left-side variance, right-side variance and feedback gain of the Gaussian function in the jth term of the ith input linguistic variable e_i, respectively, and m is the total number of the linguistic variables with respect to the input nodes. It is clear that the feedback gain contains the memory terms ϕ_{ij}^{p} which denotes the output signal of layer 2 in the previous time.

Layer 3 - Rule layer: According to the fuzzy AND operation by the algebraic product, the firing strength of the kth rule is calculated by (Lin and Lee, 1996)

$$\Phi_k(\mathbf{c}_k, \sigma_k^{\mathbf{l}}, \sigma_k^{\mathbf{r}}, \theta_k) = \prod_{i=1}^{2} \phi_{ik}\,,\ k = 1, 2, \ldots, m \tag{9}$$

where $\mathbf{c}_k = [c_{1k}\ c_{2k}]^T$, $\boldsymbol{\sigma}_k^{\mathbf{l}} = [\sigma_{1k}^{l}\ \sigma_{2k}^{l}]^T$, $\boldsymbol{\sigma}_k^{\mathbf{r}} = [\sigma_{1k}^{r}\ \sigma_{2k}^{r}]^T$ and $\boldsymbol{\theta}_k = [\theta_{1k}\ \theta_{2k}]^T$.

Layer 4 - TSK layer: The TSK layer represents the linear combination function in the consequent part of the fuzzy system. Each node in this layer is denoted by (Juang and Lo, 2008)

$$u_k = \alpha_{k0} + \alpha_{k1} e_1 + \alpha_{k2} e_2 = \alpha_k^T \xi \tag{10}$$

where $\boldsymbol{\alpha}_k = [\alpha_{k0}, \alpha_{k1}, \alpha_{k2}]^T$ is the parameter vector designed by the designer and $\boldsymbol{\xi} = [1, e_1, e_2]^T$.

Layer 5 - Output layer: The output node together with links connected it act as a defuzzifier. The single node computes the overall output as the summation of all incoming signals. The output of TRFNN can be represented as

$$u_{nc} = \sum_{k=1}^{m} u_k \Phi_k(\mathbf{c}_k, \sigma_k^{\mathbf{l}}, \sigma_k^{\mathbf{r}}, \theta_k)\,. \tag{11}$$

Then, the output of TRFNN can be represents in a vector form as

$$u_{nc} = \boldsymbol{\alpha}^T \boldsymbol{\Phi}(\mathbf{c}, \boldsymbol{\sigma}_{\mathbf{l}}, \boldsymbol{\sigma}_{\mathbf{r}}, \boldsymbol{\theta}) \tag{12}$$

where $\boldsymbol{\alpha} = [\boldsymbol{\alpha}_1^T, \ldots, \boldsymbol{\alpha}_m^T]^T$, $\boldsymbol{\Phi} = [\Phi_1 \boldsymbol{\xi}^T, \ldots, \Phi_m \boldsymbol{\xi}^T]^T$, $\mathbf{c} = [\mathbf{c}_1^T, \ldots, \mathbf{c}_m^T]^T$, $\boldsymbol{\sigma}_{\mathbf{l}} = [\boldsymbol{\sigma}_i^{\mathbf{l}T}, \ldots, \boldsymbol{\sigma}_m^{\mathbf{l}T}]^T$, $\boldsymbol{\sigma}_{\mathbf{r}} = [\boldsymbol{\sigma}_i^{\mathbf{r}T}, \ldots, \boldsymbol{\sigma}_m^{\mathbf{r}T}]^T$ and $\boldsymbol{\theta} = [\boldsymbol{\theta}_1^T, \ldots, \boldsymbol{\theta}_m^T]^T$.

In this paper, the TRFNN is used to online mimic an ideal controller. By the approximation property, an ideal TRFNN can be obtained as (Cheng *et al.*, 2007)

$$u^* = \boldsymbol{\alpha}^{*T} \boldsymbol{\Phi}(\mathbf{c}^*, \boldsymbol{\sigma}_{\mathbf{l}}^*, \boldsymbol{\sigma}_{\mathbf{r}}^*, \boldsymbol{\theta}^*) + \Delta = \boldsymbol{\alpha}^{*T} \boldsymbol{\Phi}^* + \Delta \tag{13}$$

where Δ is the approximation error, $\boldsymbol{\alpha}^*$ and $\boldsymbol{\Phi}^*$ are the optimal parameter vectors of $\boldsymbol{\alpha}$ and $\boldsymbol{\Phi}$, respectively, and $\mathbf{c}^*$, $\boldsymbol{\sigma}_{\mathbf{l}}^*$, $\boldsymbol{\sigma}_r^*$ and $\boldsymbol{\theta}^*$ are the optimal parameter vectors of $\mathbf{c}$, $\boldsymbol{\sigma}_{\mathbf{l}}$, $\boldsymbol{\sigma}_{\mathbf{r}}$ and $\boldsymbol{\theta}$, respectively. In fact, the optimal parameter vectors that are needed to best approximation cannot be determined. An estimation TRFNN is defined as

$$\hat{u}_{nc} = \hat{\boldsymbol{\alpha}}^T \boldsymbol{\Phi}(\hat{\mathbf{c}}, \hat{\boldsymbol{\sigma}}_{\mathbf{l}}, \hat{\boldsymbol{\sigma}}_{\mathbf{r}}, \hat{\boldsymbol{\theta}}) = \hat{\boldsymbol{\alpha}}^T \hat{\boldsymbol{\Phi}} \tag{14}$$

where $\hat{\boldsymbol{\alpha}}$ and $\hat{\boldsymbol{\Phi}}$ are the estimated parameter vectors of $\boldsymbol{\alpha}$ and $\boldsymbol{\Phi}$, respectively, and $\hat{\mathbf{c}}$, $\hat{\boldsymbol{\sigma}}_{\mathbf{l}}$, $\hat{\boldsymbol{\sigma}}_{\mathbf{r}}$ and $\hat{\boldsymbol{\theta}}$ are the estimated parameter vectors of $\mathbf{c}$, $\boldsymbol{\sigma}_{\mathbf{l}}$, $\boldsymbol{\sigma}_{\mathbf{r}}$ and $\boldsymbol{\theta}$, respectively. To speed up the convergence, the optimal parameter vector $\boldsymbol{\alpha}^*$ is decomposed into two parts as (Golea *et al.*, 2002; Hsu *et al.*, 2009)

$$\boldsymbol{\alpha}^{*} = \eta_P \boldsymbol{\alpha}_{\mathbf{P}}^{*} + \eta_I \boldsymbol{\alpha}_{\mathbf{I}}^{*} \tag{15}$$

where $\boldsymbol{\alpha}_{\mathbf{P}}^{*}$ and $\boldsymbol{\alpha}_{\mathbf{I}}^{*}$ are the proportional and integral terms of $\boldsymbol{\sigma}^{*}$, respectively, η_P and η_I are positive coefficients, and $\boldsymbol{\alpha}_{\mathbf{I}}^{*} = \int_0^t \boldsymbol{\alpha}_{\mathbf{P}}^{*} \, d\tau$. Similarly, the estimation parameter vector $\hat{\boldsymbol{\alpha}}$ is decomposed into two parts as (Golea *et al.*, 2002; Hsu *et al.*, 2009)

$$\hat{\boldsymbol{\alpha}} = \eta_P \hat{\boldsymbol{\alpha}}_{\mathbf{P}} + \eta_I \hat{\boldsymbol{\alpha}}_{\mathbf{I}} \tag{16}$$

where $\hat{\boldsymbol{\alpha}}_{\mathbf{P}}$ and $\hat{\boldsymbol{\alpha}}_{\mathbf{I}}$ are the proportional and integral terms of $\hat{\boldsymbol{\alpha}}$, respectively, and $\hat{\boldsymbol{\alpha}}_{\mathbf{I}} = \int_0^t \hat{\boldsymbol{\alpha}}_{\mathbf{P}} \, d\tau$. Thus, $\tilde{\boldsymbol{\alpha}} = \boldsymbol{\alpha}^{*} - \hat{\boldsymbol{\alpha}}$ can be expressed as

$$\tilde{\boldsymbol{\alpha}} = \eta_I \tilde{\boldsymbol{\alpha}}_{\mathbf{I}} - \eta_P \hat{\boldsymbol{\alpha}}_{\mathbf{P}} + \eta_P \boldsymbol{\alpha}_{\mathbf{P}}^{*} \tag{17}$$

where $\tilde{\boldsymbol{\alpha}}_{\mathbf{I}} = \boldsymbol{\alpha}_{\mathbf{I}}^{*} - \hat{\boldsymbol{\alpha}}_{\mathbf{I}}$. Then, the estimation error is obtained as

$$\begin{aligned}
\tilde{u} &= u^{*} - \hat{u}_{nc} \\
&= \boldsymbol{\alpha}^{*T} \boldsymbol{\Phi}^{*} + \Delta - \hat{\boldsymbol{\alpha}}^{T} \hat{\boldsymbol{\Phi}} \\
&= \tilde{\boldsymbol{\alpha}}^{T} \hat{\boldsymbol{\Phi}} + \hat{\boldsymbol{\alpha}}^{T} \tilde{\boldsymbol{\Phi}} + \tilde{\boldsymbol{\alpha}}^{T} \tilde{\boldsymbol{\Phi}} + \Delta \\
&= (\eta_I \tilde{\boldsymbol{\alpha}}_{\mathbf{I}} - \eta_P \hat{\boldsymbol{\alpha}}_{\mathbf{P}} + \eta_P \boldsymbol{\alpha}_{\mathbf{P}}^{*})^{T} \hat{\boldsymbol{\Phi}} + \hat{\boldsymbol{\alpha}}^{T} \tilde{\boldsymbol{\Phi}} + \tilde{\boldsymbol{\alpha}}^{T} \tilde{\boldsymbol{\Phi}} + \Delta \\
&= \eta_I \tilde{\boldsymbol{\alpha}}_{\mathbf{I}}^{T} \hat{\boldsymbol{\Phi}} - \eta_P \hat{\boldsymbol{\alpha}}_{\mathbf{P}}^{T} \hat{\boldsymbol{\Phi}} + \eta_P \boldsymbol{\alpha}_{\mathbf{P}}^{*T} \hat{\boldsymbol{\Phi}} + \hat{\boldsymbol{\alpha}}^{T} \tilde{\boldsymbol{\Phi}} + \tilde{\boldsymbol{\alpha}}^{T} \tilde{\boldsymbol{\Phi}} + \Delta
\end{aligned} \tag{18}$$

where $\tilde{\boldsymbol{\alpha}} = \boldsymbol{\alpha}^{*} - \hat{\boldsymbol{\alpha}}$ and $\tilde{\boldsymbol{\Phi}} = \boldsymbol{\Phi}^{*} - \hat{\boldsymbol{\Phi}}$. The Taylor expansion linearization technique is employed to transform the nonlinear function into a partially linear form, i.e. (Cheng *et al.*, 2007)

$$\tilde{\boldsymbol{\Phi}} = \boldsymbol{\Phi}_{\mathbf{c}}^{T} \tilde{\mathbf{c}} + \boldsymbol{\Phi}_{\mathbf{l}}^{T} \tilde{\boldsymbol{\sigma}}_{\mathbf{l}} + \boldsymbol{\Phi}_{\mathbf{r}}^{T} \tilde{\boldsymbol{\sigma}}_{\mathbf{r}} + \boldsymbol{\Phi}_{\boldsymbol{\theta}}^{T} \tilde{\boldsymbol{\theta}} + \mathbf{h} \tag{19}$$

where $\tilde{\mathbf{c}} = \mathbf{c}^{*} - \hat{\mathbf{c}}$, $\tilde{\boldsymbol{\sigma}}_{\mathbf{l}} = \boldsymbol{\sigma}_{\mathbf{l}}^{*} - \hat{\boldsymbol{\sigma}}_{\mathbf{l}}$, $\tilde{\boldsymbol{\sigma}}_{\mathbf{r}} = \boldsymbol{\sigma}_{\mathbf{r}}^{*} - \hat{\boldsymbol{\sigma}}_{\mathbf{r}}$, $\tilde{\boldsymbol{\theta}} = \boldsymbol{\theta}^{*} - \hat{\boldsymbol{\theta}}$, $\mathbf{h}$ is a vector of high order terms, $\boldsymbol{\Phi}_{\mathbf{c}} = \left[\frac{\partial \Phi_1}{\partial \mathbf{c}} \cdots \frac{\partial \Phi_m}{\partial \mathbf{c}} \right] \Big|_{\mathbf{c}=\hat{\mathbf{c}}}$, $\boldsymbol{\Phi}_{\mathbf{l}} = \left[\frac{\partial \Phi_1}{\partial \boldsymbol{\sigma}_{\mathbf{l}}} \cdots \frac{\partial \Phi_m}{\partial \boldsymbol{\sigma}_{\mathbf{l}}} \right] \Big|_{\boldsymbol{\sigma}_{\mathbf{l}}=\hat{\boldsymbol{\sigma}}_{\mathbf{l}}}$, $\boldsymbol{\Phi}_{\mathbf{r}} = \left[\frac{\partial \Phi_1}{\partial \boldsymbol{\sigma}_{\mathbf{r}}} \cdots \frac{\partial \Phi_m}{\partial \boldsymbol{\sigma}_{\mathbf{r}}} \right] \Big|_{\boldsymbol{\sigma}_{\mathbf{r}}=\hat{\boldsymbol{\sigma}}_{\mathbf{r}}}$, and $\boldsymbol{\Phi}_{\boldsymbol{\theta}} = \left[\frac{\partial \Phi_1}{\partial \boldsymbol{\theta}} \cdots \frac{\partial \Phi_m}{\partial \boldsymbol{\theta}} \right] \Big|_{\boldsymbol{\theta}=\hat{\boldsymbol{\theta}}}$. Substitute (19) into (18) yields

$$\begin{aligned}
\tilde{u} &= \eta_I \tilde{\boldsymbol{\alpha}}_{\mathbf{I}}^{T} \hat{\boldsymbol{\Phi}} - \eta_P \hat{\boldsymbol{\alpha}}_{\mathbf{P}}^{T} \hat{\boldsymbol{\Phi}} + \eta_P \boldsymbol{\alpha}_{\mathbf{P}}^{*T} \hat{\boldsymbol{\Phi}} + \hat{\boldsymbol{\alpha}}^{T} (\boldsymbol{\Phi}_{\mathbf{c}}^{T} \tilde{\mathbf{c}} + \boldsymbol{\Phi}_{\mathbf{l}}^{T} \tilde{\boldsymbol{\sigma}}_{\mathbf{l}} + \boldsymbol{\Phi}_{\mathbf{r}}^{T} \tilde{\boldsymbol{\sigma}}_{\mathbf{r}} + \boldsymbol{\Phi}_{\boldsymbol{\theta}}^{T} \tilde{\boldsymbol{\theta}} + \mathbf{h}) + \tilde{\boldsymbol{\alpha}}^{T} \tilde{\boldsymbol{\Phi}} + \Delta \\
&= \eta_I \tilde{\boldsymbol{\alpha}}_{\mathbf{I}}^{T} \hat{\boldsymbol{\Phi}} - \eta_P \hat{\boldsymbol{\alpha}}_{\mathbf{P}}^{T} \hat{\boldsymbol{\Phi}} + \tilde{\mathbf{c}}^{T} \boldsymbol{\Phi}_{\mathbf{c}} \hat{\boldsymbol{\alpha}} + \tilde{\boldsymbol{\sigma}}_{\mathbf{l}}^{T} \boldsymbol{\Phi}_{\mathbf{l}} \hat{\boldsymbol{\alpha}} + \tilde{\boldsymbol{\sigma}}_{\mathbf{r}}^{T} \boldsymbol{\Phi}_{\mathbf{r}} \hat{\boldsymbol{\alpha}} + \tilde{\boldsymbol{\theta}}^{T} \boldsymbol{\Phi}_{\boldsymbol{\theta}} \hat{\boldsymbol{\alpha}} + \varepsilon
\end{aligned} \tag{20}$$

where $\hat{\boldsymbol{\alpha}}^{T} \boldsymbol{\Phi}_{\mathbf{c}}^{T} \tilde{\mathbf{c}} = \tilde{\mathbf{c}}^{T} \boldsymbol{\Phi}_{\mathbf{c}} \hat{\boldsymbol{\alpha}}$, $\hat{\boldsymbol{\alpha}}^{T} \boldsymbol{\Phi}_{\mathbf{l}}^{T} \tilde{\boldsymbol{\sigma}}_{\mathbf{l}} = \tilde{\boldsymbol{\sigma}}_{\mathbf{l}}^{T} \boldsymbol{\Phi}_{\mathbf{l}} \hat{\boldsymbol{\alpha}}$, $\hat{\boldsymbol{\alpha}}^{T} \boldsymbol{\Phi}_{\mathbf{r}}^{T} \tilde{\boldsymbol{\sigma}}_{\mathbf{r}} = \tilde{\boldsymbol{\sigma}}_{\mathbf{r}}^{T} \boldsymbol{\Phi}_{\mathbf{r}} \hat{\boldsymbol{\alpha}}$ and $\hat{\boldsymbol{\alpha}}^{T} \boldsymbol{\Phi}_{\boldsymbol{\theta}}^{T} \tilde{\boldsymbol{\theta}} = \tilde{\boldsymbol{\theta}}^{T} \boldsymbol{\Phi}_{\boldsymbol{\theta}} \hat{\boldsymbol{\alpha}}$ are used since they are scalars and $\varepsilon = \eta_P \boldsymbol{\alpha}_{\mathbf{P}}^{*T} \hat{\boldsymbol{\Phi}} + \hat{\boldsymbol{\alpha}}^{\mathrm{T}} \mathbf{h} + \tilde{\boldsymbol{\alpha}}^{T} \tilde{\boldsymbol{\Phi}} + \Delta$ denotes the lump of approximation error and is assumed to be bounded by $|\varepsilon| \le E$.

(B) Design of the ATRFNC System

Substituting (7) into (4), the error dynamic equation can be obtained as

$$\dot{\mathbf{e}} = \mathbf{A}\mathbf{e} + \mathbf{b}[z(\mathbf{x}) - \hat{u}_{nc} - u_{rc}]. \tag{21}$$

Substituting (5) into (21) and using approximation error equation (20), (21) can be rewritten as

$$\begin{aligned}\dot{\mathbf{e}} &= (\mathbf{A}-\mathbf{bk})\mathbf{e}+\mathbf{b}(u^{*}-\hat{u}_{nc}-u_{rc})\\ &= \mathbf{\Lambda e}+\mathbf{b}(\eta_I\tilde{\boldsymbol{\alpha}}_{\mathbf{I}}^{T}\hat{\mathbf{\Phi}}-\eta_P\hat{\boldsymbol{\alpha}}_{\mathbf{P}}^{T}\hat{\mathbf{\Phi}}+\tilde{\mathbf{c}}^{T}\mathbf{\Phi}_{\mathbf{c}}\hat{\boldsymbol{\alpha}}+\tilde{\boldsymbol{\sigma}}_{\mathbf{l}}^{T}\mathbf{\Phi}_{\mathbf{l}}\hat{\boldsymbol{\alpha}}+\tilde{\boldsymbol{\sigma}}_{\mathbf{r}}^{T}\mathbf{\Phi}_{\mathbf{r}}\hat{\boldsymbol{\alpha}}+\tilde{\boldsymbol{\theta}}^{T}\mathbf{\Phi}_{\boldsymbol{\theta}}\hat{\boldsymbol{\alpha}}+\varepsilon-u_{rc}).\end{aligned} \tag{22}$$

In this paper, the robust compensator is designed as

$$u_{rc}=\hat{\varepsilon}+K\mathbf{e}^{T}\mathbf{Pb} \tag{23}$$

where $\hat{\varepsilon}$ denotes the estimated value of the approximation error and K is a small positive constant. Substituting (23) into (22) yields

$$\dot{\mathbf{e}}=\mathbf{\Lambda e}+\mathbf{b}(\eta_I\tilde{\boldsymbol{\alpha}}_{\mathbf{I}}^{T}\hat{\mathbf{\Phi}}-\eta_P\hat{\boldsymbol{\alpha}}_{\mathbf{P}}^{T}\hat{\mathbf{\Phi}}+\tilde{\mathbf{c}}^{T}\mathbf{\Phi}_{\mathbf{c}}\hat{\boldsymbol{\alpha}}+\tilde{\boldsymbol{\sigma}}_{\mathbf{l}}^{T}\mathbf{\Phi}_{\mathbf{l}}\hat{\boldsymbol{\alpha}}+\tilde{\boldsymbol{\sigma}}_{\mathbf{r}}^{T}\mathbf{\Phi}_{\mathbf{r}}\hat{\boldsymbol{\alpha}}+\tilde{\boldsymbol{\theta}}^{T}\mathbf{\Phi}_{\boldsymbol{\theta}}\hat{\boldsymbol{\alpha}}+\tilde{\varepsilon}-K\mathbf{e}^{T}\mathbf{Pb}) \tag{24}$$

where $\tilde{\varepsilon}=\varepsilon-\hat{\varepsilon}$. To guarantee the stability of the proposed ATRFNC system, a Lyapunov function is defined as

$$V=\frac{1}{2}\mathbf{e}^{T}\mathbf{Pe}+\frac{\eta_I}{2}\tilde{\boldsymbol{\alpha}}_{\mathbf{I}}^{T}\tilde{\boldsymbol{\alpha}}_{\mathbf{I}}+\frac{\tilde{\mathbf{c}}^{T}\tilde{\mathbf{c}}}{2\eta_c}+\frac{\tilde{\boldsymbol{\sigma}}_{\mathbf{l}}^{T}\tilde{\boldsymbol{\sigma}}_{\mathbf{l}}}{2\eta_l}+\frac{\tilde{\boldsymbol{\sigma}}_{\mathbf{r}}^{T}\tilde{\boldsymbol{\sigma}}_{\mathbf{r}}}{2\eta_r}+\frac{\tilde{\boldsymbol{\theta}}^{T}\tilde{\boldsymbol{\theta}}}{2\eta_\theta}+\frac{\tilde{\varepsilon}^{2}}{2\eta_\varepsilon} \tag{25}$$

where η_c, η_I, η_r, η_θ and η_ε are the positive learning rates and $\mathbf{P}$ is a symmetric positive definite matrix that satisfies the equation

$$\Lambda^{T}\mathbf{P}+\mathbf{P}\Lambda=-\mathbf{Q} \tag{26}$$

in which $\mathbf{Q}$ is a positive definite matrix. Taking the derivative of Lyapunov function in (25) and using (24) yield

$$\begin{aligned}\dot{V}&=\frac{1}{2}\dot{\mathbf{e}}^{T}\mathbf{Pe}+\frac{1}{2}\mathbf{e}^{T}\mathbf{P}\dot{\mathbf{e}}+\eta_I\tilde{\boldsymbol{\alpha}}_{\mathbf{I}}^{T}\dot{\tilde{\boldsymbol{\alpha}}}_{\mathbf{I}}+\frac{\tilde{\mathbf{c}}^{T}\dot{\tilde{\mathbf{c}}}}{\eta_c}+\frac{\tilde{\boldsymbol{\sigma}}_{\mathbf{l}}^{T}\dot{\tilde{\boldsymbol{\sigma}}}_{\mathbf{l}}}{\eta_l}+\frac{\tilde{\boldsymbol{\sigma}}_{\mathbf{r}}^{T}\dot{\tilde{\boldsymbol{\sigma}}}_{\mathbf{r}}}{\eta_r}+\frac{\tilde{\boldsymbol{\theta}}^{T}\dot{\tilde{\boldsymbol{\theta}}}}{\eta_\theta}+\frac{\tilde{\varepsilon}\dot{\tilde{\varepsilon}}}{\eta_\varepsilon}\\ &=\frac{-1}{2}\mathbf{e}^{T}\mathbf{Qe}+\mathbf{e}^{T}\mathbf{Pb}(\eta_I\tilde{\boldsymbol{\alpha}}_{\mathbf{I}}^{T}\hat{\mathbf{\Phi}}-\eta_P\hat{\boldsymbol{\alpha}}_{\mathbf{P}}^{T}\hat{\mathbf{\Phi}}+\tilde{\mathbf{c}}^{T}\mathbf{\Phi}_{\mathbf{c}}\hat{\boldsymbol{\alpha}}+\tilde{\boldsymbol{\sigma}}_{\mathbf{l}}^{T}\mathbf{\Phi}_{\mathbf{l}}\hat{\boldsymbol{\alpha}}+\tilde{\boldsymbol{\sigma}}_{\mathbf{r}}^{T}\mathbf{\Phi}_{\mathbf{r}}\hat{\boldsymbol{\alpha}}+\tilde{\boldsymbol{\theta}}^{T}\mathbf{\Phi}_{\boldsymbol{\theta}}\hat{\boldsymbol{\alpha}}\\ &\quad+\tilde{\varepsilon}-K\mathbf{e}^{T}\mathbf{Pb})+\eta_I\tilde{\boldsymbol{\alpha}}_{\mathbf{I}}^{T}\dot{\tilde{\boldsymbol{\alpha}}}_{\mathbf{I}}+\frac{\tilde{\mathbf{c}}^{T}\dot{\tilde{\mathbf{c}}}}{\eta_c}+\frac{\tilde{\boldsymbol{\sigma}}_{\mathbf{l}}^{T}\dot{\tilde{\boldsymbol{\sigma}}}_{\mathbf{l}}}{\eta_l}+\frac{\tilde{\boldsymbol{\sigma}}_{\mathbf{r}}^{T}\dot{\tilde{\boldsymbol{\sigma}}}_{\mathbf{r}}}{\eta_r}+\frac{\tilde{\boldsymbol{\theta}}^{T}\dot{\tilde{\boldsymbol{\theta}}}}{\eta_\theta}+\frac{\tilde{\varepsilon}\dot{\tilde{\varepsilon}}}{\eta_\varepsilon}\\ &=\frac{-1}{2}\mathbf{e}^{T}\mathbf{Qe}-\eta_P\mathbf{e}^{T}\mathbf{Pb}\hat{\boldsymbol{\alpha}}_{\mathbf{P}}^{T}\hat{\mathbf{\Phi}}+\eta_I\tilde{\boldsymbol{\alpha}}_{\mathbf{I}}^{T}(\mathbf{e}^{T}\mathbf{Pb}\hat{\mathbf{\Phi}}+\dot{\tilde{\boldsymbol{\alpha}}}_{\mathbf{I}})+\tilde{\mathbf{c}}^{T}(\mathbf{e}^{T}\mathbf{Pb}\mathbf{\Phi}_{\mathbf{c}}\hat{\boldsymbol{\alpha}}+\frac{\dot{\tilde{\mathbf{c}}}}{\eta_c})\\ &\quad+\tilde{\boldsymbol{\sigma}}_{\mathbf{l}}^{T}(\mathbf{e}^{T}\mathbf{Pb}\mathbf{\Phi}_{\mathbf{l}}\hat{\boldsymbol{\alpha}}+\frac{\dot{\tilde{\boldsymbol{\sigma}}}_{\mathbf{l}}}{\eta_l})+\tilde{\boldsymbol{\sigma}}_{\mathbf{r}}^{T}(\mathbf{e}^{T}\mathbf{Pb}\mathbf{\Phi}_{\mathbf{r}}\hat{\boldsymbol{\alpha}}+\frac{\dot{\tilde{\boldsymbol{\sigma}}}_{\mathbf{r}}}{\eta_r})+\tilde{\boldsymbol{\theta}}^{T}(\mathbf{e}^{T}\mathbf{Pb}\mathbf{\Phi}_{\boldsymbol{\theta}}\hat{\boldsymbol{\alpha}}+\frac{\dot{\tilde{\boldsymbol{\theta}}}}{\eta_\theta})\\ &\quad+\tilde{\varepsilon}(\mathbf{e}^{T}\mathbf{Pb}+\frac{\dot{\tilde{\varepsilon}}}{\eta_\varepsilon})-K(\mathbf{e}^{T}\mathbf{Pb})^{2}.\end{aligned} \tag{27}$$

If the adaptation laws are chosen as

$$\hat{\boldsymbol{\alpha}}_{\mathbf{P}}=\mathbf{e}^{T}\mathbf{Pb}\hat{\mathbf{\Phi}} \tag{28}$$

$$\dot{\hat{\boldsymbol{\alpha}}}_{\mathbf{I}}=-\dot{\tilde{\boldsymbol{\alpha}}}_{\mathbf{I}}=\mathbf{e}^{T}\mathbf{Pb}\hat{\mathbf{\Phi}} \tag{29}$$

$$\dot{\hat{\mathbf{c}}} = -\dot{\tilde{\mathbf{c}}} = \eta_c \mathbf{e}^T \mathbf{Pb} \mathbf{\Phi}_\mathbf{c} \hat{\boldsymbol{\alpha}} \tag{30}$$

$$\dot{\hat{\boldsymbol{\sigma}}}_\mathbf{l} = -\dot{\tilde{\boldsymbol{\sigma}}}_\mathbf{l} = \eta_l \mathbf{e}^T \mathbf{Pb} \mathbf{\Phi}_\mathbf{l} \hat{\boldsymbol{\alpha}} \tag{31}$$

$$\dot{\hat{\boldsymbol{\sigma}}}_\mathbf{r} = -\dot{\tilde{\boldsymbol{\sigma}}}_\mathbf{r} = \eta_r \mathbf{e}^T \mathbf{Pb} \mathbf{\Phi}_\mathbf{r} \hat{\boldsymbol{\alpha}} \tag{32}$$

$$\dot{\hat{\boldsymbol{\theta}}} = -\dot{\tilde{\boldsymbol{\theta}}} = \eta_\theta \mathbf{e}^T \mathbf{Pb} \mathbf{\Phi}_\boldsymbol{\theta} \hat{\boldsymbol{\alpha}} \tag{33}$$

$$\dot{\hat{\varepsilon}} = -\dot{\tilde{\varepsilon}} = \eta_\varepsilon \mathbf{e}^T \mathbf{Pb} \tag{34}$$

then (27) can be rewritten as

$$\dot{V} = \frac{-1}{2} \mathbf{e}^T \mathbf{Q} \mathbf{e} - \eta_P \hat{\boldsymbol{\alpha}}_\mathbf{P}^T \hat{\boldsymbol{\alpha}}_\mathbf{P} - K(\mathbf{e}^T \mathbf{Pb})^2$$

$$\leq \frac{-1}{2} \mathbf{e}^T \mathbf{Q} \mathbf{e} \leq 0 . \tag{35}$$

That is, $\mathbf{e}(t) \to 0$ as $t \to \infty$ (Slotine and Li, 1991). As a result, the stability of the proposed ATRFNC system can be guaranteed.

IV. SIMULATION RESULTS

It should be emphasized that the development of the ATRFNC system doesn't need to know the system dynamics of the controlled plant. The controller parameters of the ATRFNC system can be online tuned by the proposed adaptive laws. To investigate the effectiveness of the proposed ATRFNC system, a comparison among the supervisory recurrent fuzzy neural network control (Lin and Hsu, 2004), the adaptive recurrent-neural-network control (Lin *et al.*, 2006) and the proposed ATRFNC system is made.

First, the supervisory recurrent fuzzy neural network control (Lin and Hsu, 2004) is applied to the coupled neurons. The simulation results of the supervisory recurrent fuzzy neural network control system are shown in Figs. 6 and 7 for $g = 0.01$ and $g = 1.0$, respectively. The phase portraits on plan of $X_1 - Y_1$ are shown in Figs. 6(a) and 7(a), the phase portraits on plan of $X_2 - Y_2$ are shown in Figs. 6(b) and 7(b), the phase portraits on plan of $X_1 - X_2$ are shown in Figs. 6(c) and 7(c), and the phase portraits on plan of Y_1–Y_2 are shown in Figs. 6(d) and 7(d), the time responses of error e_1 are shown in Figs. 6(e) and 7(e), the time responses of error e_2 are shown in Figs. 6(f) and 7(f), and the associated control effort are shown in Figs. 6(g) and 7(g). The simulation results show that the synchronization can be obtained by the supervisory recurrent fuzzy neural network control system. Unfortunately, to guarantee the system stability, a switching compensator should be used, but the undesirable chattering phenomenon occurs as shown in Figs. 5(g) and 6(g).

Then, the adaptive recurrent-neural-network control (Lin *et al.*, 2006) is applied to the coupled neurons again. The simulation results of the adaptive recurrent-neural-network control system are shown in Figs. 8 and 9 for $g = 0.01$ and $g = 1.0$, respectively. The phase portraits on plan of X_1–Y_1 are shown in Figs. 8(a) and 9(a), the phase portraits on plan of $X_2 - Y_2$ are shown in Figs. 8(b) and 9(b), the phase portraits on plan of X_1–X_2 are shown in Figs. 8(c) and 9(c), and the phase portraits on plan of $Y_1 - Y_2$ are shown in Figs. 8(d) and 9(d), the time responses of error e_1 are shown in Figs. 8(e) and 9(e), the time responses of error e_2 are shown in Figs. 8(f) and 9(f), and the associated control effort are shown in Figs. 8(g) and 9(g). The simulation results show that the synchronization can be obtained by the adaptive recurrent-neural-network control. Since the adaptation laws of the adaptive recurrent-neural-network control system are designed in an integral-type learning form, the convergence speed of the synchronization error is slow.

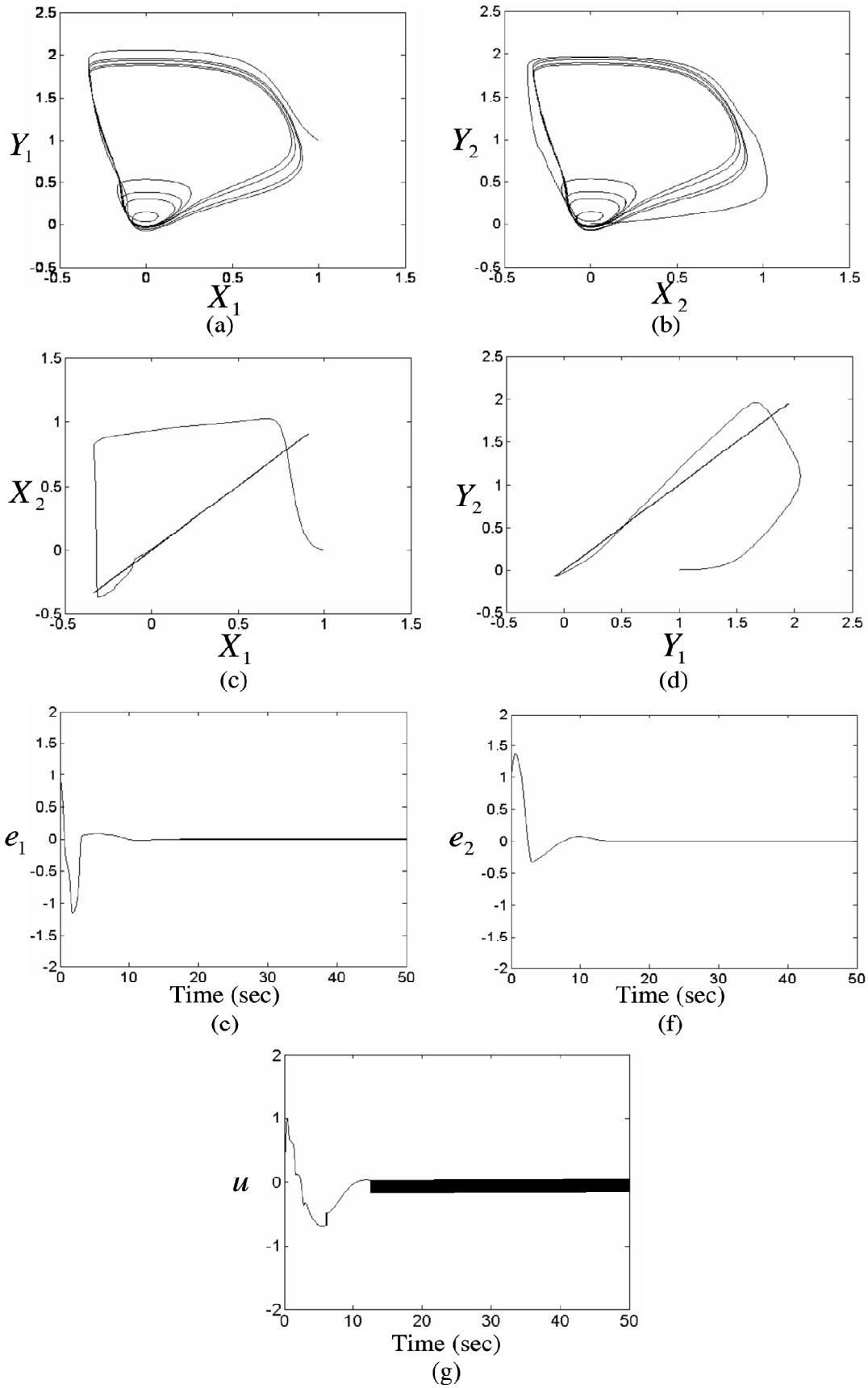

Figure 6: The Simulation Results of the Supervisory Recurrent Fuzzy Neural Network Control System for $g = 0.01$

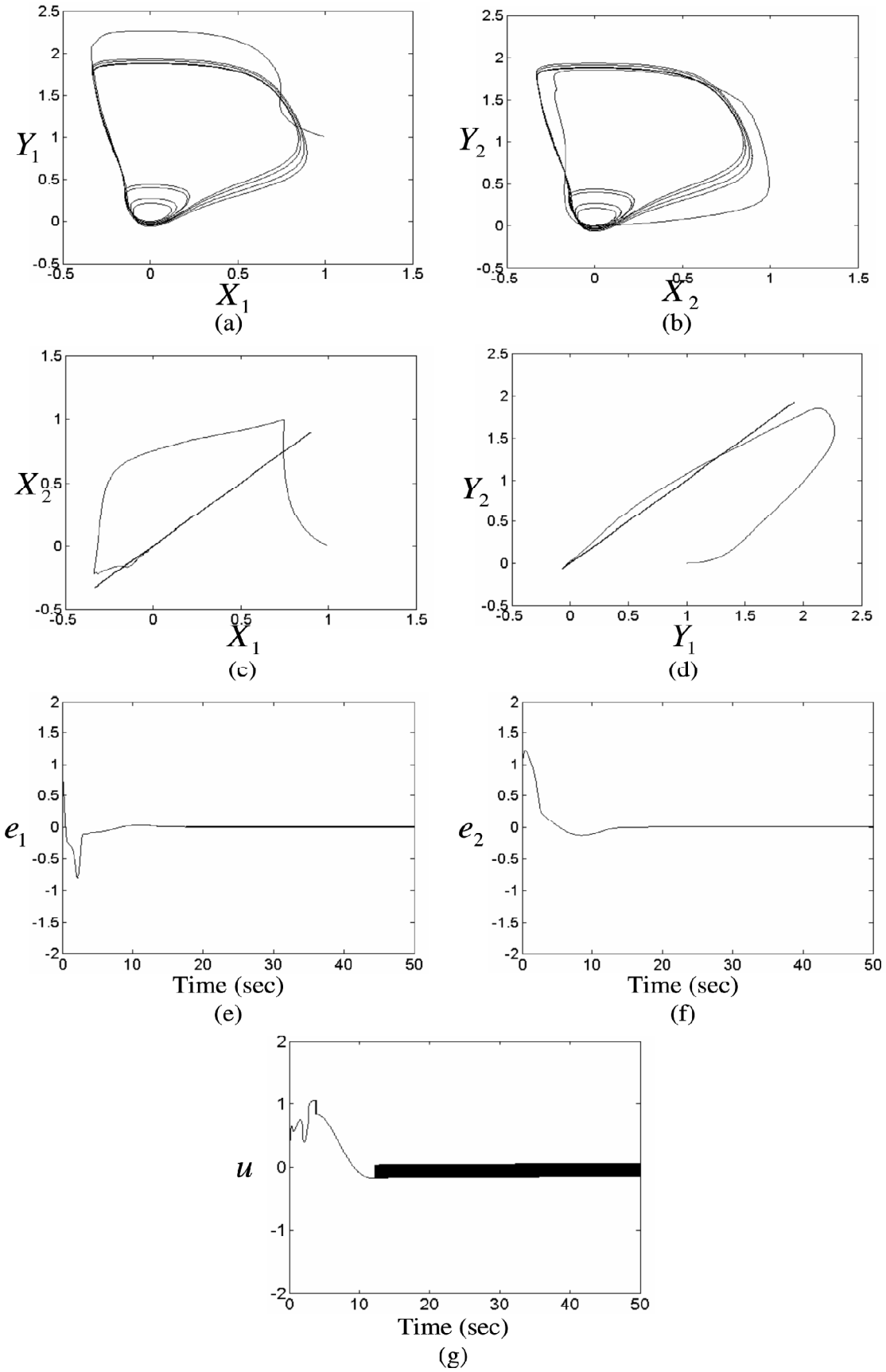

Figure 7: The Simulation Results of the Supervisory Recurrent Fuzzy Neural Network Control System for g = 1.0

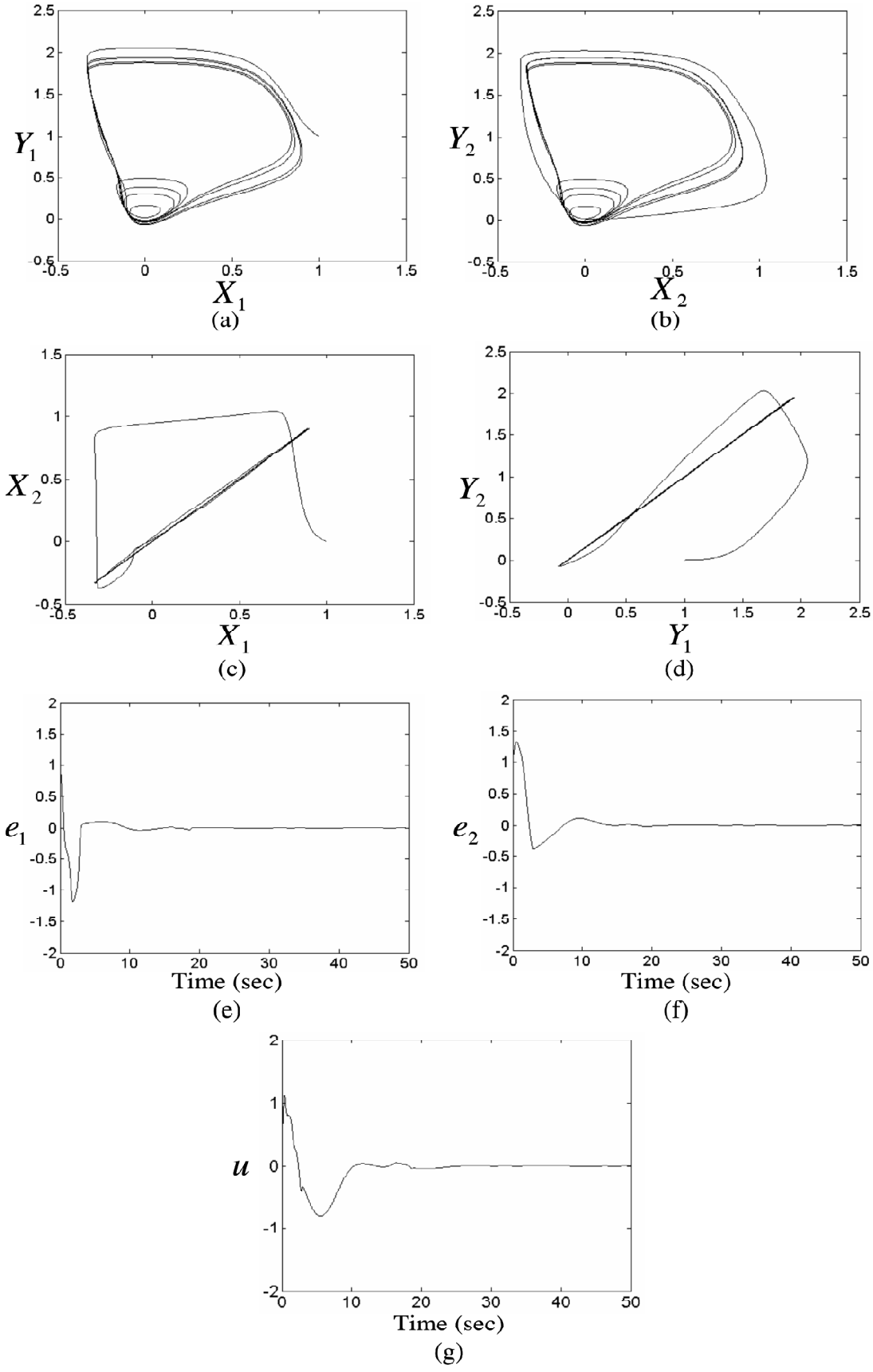

Figure 8: The Simulation Results of the ATRFNC System with Integral-type Learning Algorithm for g = 0.01

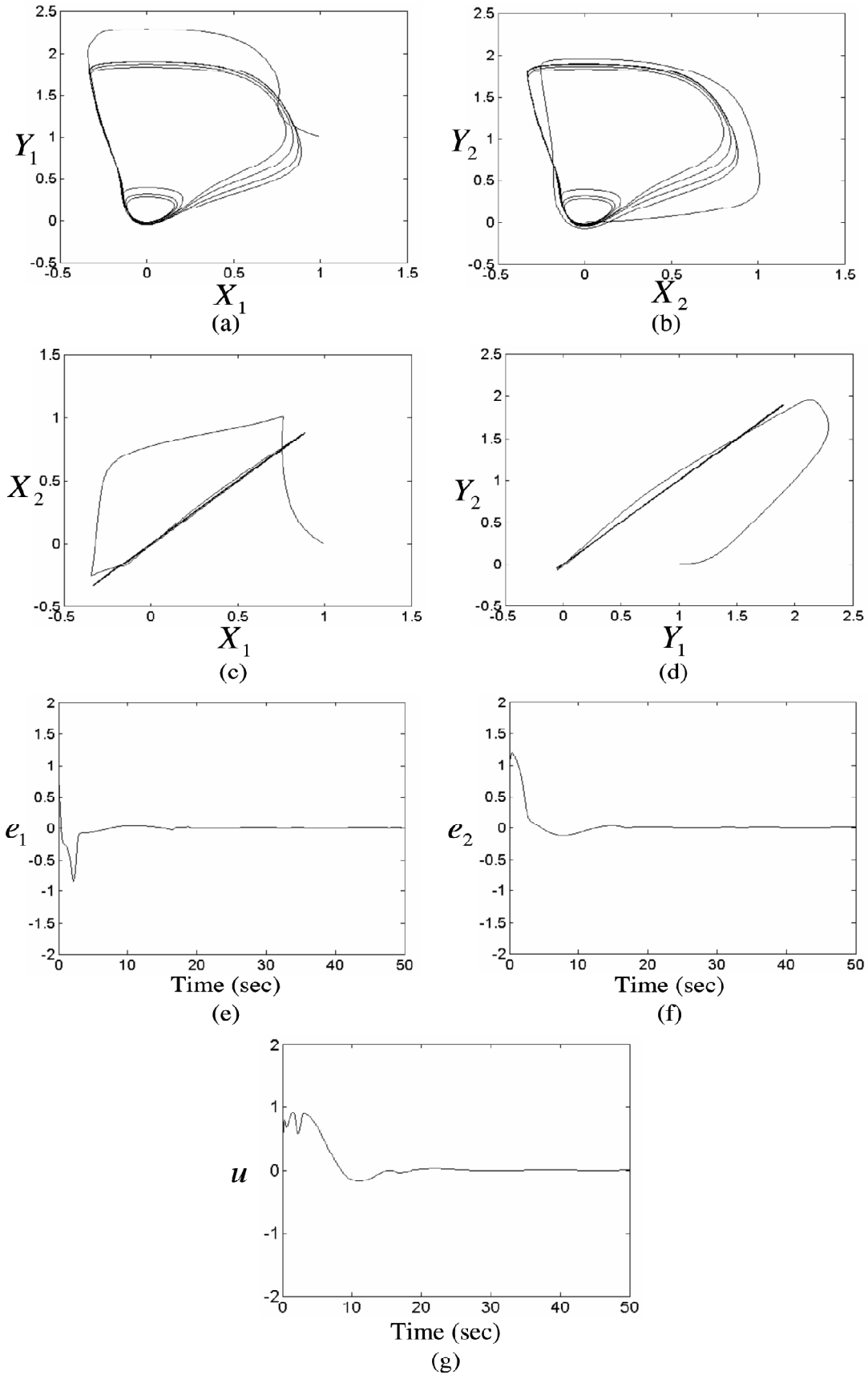

Figure 9: The Simulation Results of the ATRFNC System with Integral-type Learning Algorithm for g = 1.0

Finally, the proposed ATRFNC system is applied to the coupled neurons again. The parameters of the ATRFNC system are selected as $\eta_P = \eta_I = 10$, $\eta_c = \eta_l = \eta_r = \eta_\theta = 1$ and $\eta_\varepsilon = 0.1$. All the parameters are chosen through some trials to achieve a good transient control performance in the simulation considering the requirement of stability. The simulation results of the ATRFNC system are shown in Figs. 10 and 11 for $g = 0.01$ and $g = 1.0$, respectively. The phase portraits on plan of X_1–Y_1 are shown in Figs. 10(a) and 11(a), the phase portraits on plan of $X_2 - Y_2$ are shown in Figs. 10(b) and 11(b), the phase portraits on plan of X_1–X_2 are shown in Figs. 10(c) and 11(c), and the phase portraits on plan of Y_1–Y_2 are shown in Figs. 10(d) and 11(d), the time responses of error e_1 are shown in Figs. 10(e) and 11(e), the time responses of error e_2 are shown in Figs. 10(f) and 11(f), and the associated control effort are shown in Figs. 10(g) and 11(g). The simulation results show that the synchronization can be obtained by the proposed ATRFNC system and the synchronization errors converge quickly by using the proposed PI-type learning algorithm.

In addition, the performance measures of various control schemes are summarized in Table 1. The performance measures are shown in Tables 1(a) and 1(b) for $g = 0.01$ and $g = 1.0$, respectively. It shows that the proposed ATRFNC system possesses the most accurate synchronization performance and the synchronization errors converge quickly by using the proposed PI-type learning algorithm.

Table 1
Performance Measures

(a)

Error / *Methods*	*average*	*standard deviation*
supervisory recurrent fuzzy neural network control	0.0177	0.1689
ATRFNC system with integral-type learning algorithm	0.0160	0.1646
ATRFNC system with PI-type learning algorithm	0.0148	0.1276

(b)

Error / *Methods*	*average*	*standard deviation*
supervisory recurrent fuzzy neural network control	0.0208	0.1576
ATRFNC system with integral-type learning algorithm	0.0194	0.1527
ATRFNC system with PI-type learning algorithm	0.0175	0.1361

V. CONCLUSIONS

The weights of the output layer in the TSK-type recurrent fuzzy neural network (TRFNN) use a functional-type form, so the proposed TRFNN provides powerful representation, good generalization capability and dynamic mapping. Then, this paper has successfully developed an adaptive TSK-type recurrent fuzzy network control (ATRFNC) system with a proportional-integral (PI)-type learning algorithm. The proposed ATRFNC system is composed of a neural controller and a robust compensator. The neural controller utilizes a TRFNN to online mimic an ideal controller and the robust compensator is designed to dispel the approximation error introduced by the neural controller without occurring chattering phenomena. All the controller parameters of the proposed ATRFNC system are online tuned based on the Lyapunov stability theorem, thus the stability of the closed-loop control system can be guaranteed. Finally, a comparison among the supervisory recurrent fuzzy neural network control (Lin and Hsu, 2004), the adaptive recurrent-neural-network control (Lin *et al.*, 2006) and the proposed ATRFNC system is made. The simulation results show that the convergences of the synchronization error can be speeded up by using the developed PI-type learning algorithm.

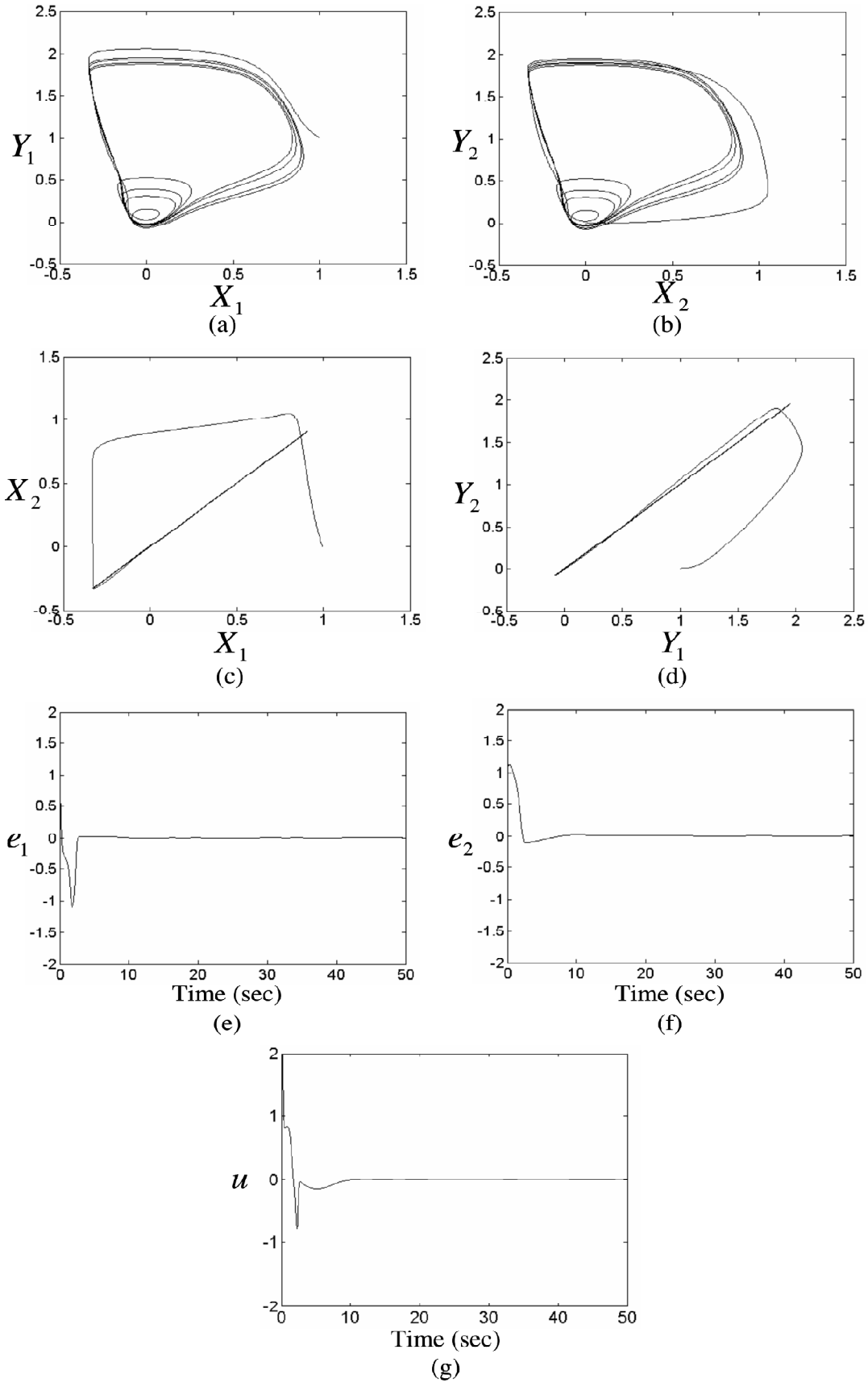

Figure 10: The Simulation Results of the ATRFNC System with PI-type Learning Algorithm for g = 0.01

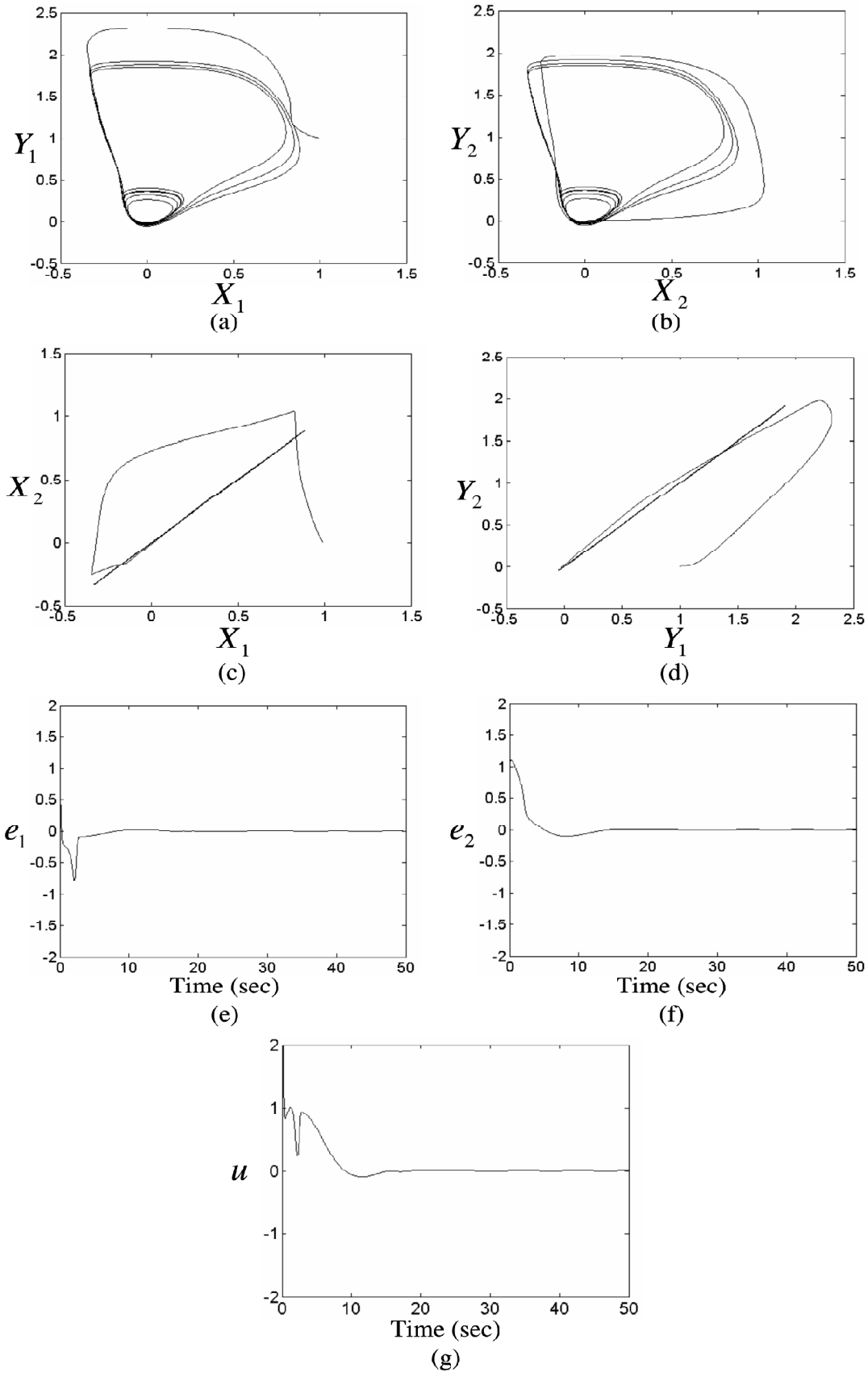

Figure 11: The Simulation Results of the ATRFNC System with PI -type Learning Algorithm for g = 1.0

Acknowledgments

The authors appreciate the partial financial support from the National Science Council of Republic of China under grant NSC 99-2628-E-216-002. The authors are grateful to the reviewers for their valuable comments.

References

[1] Chen, C. H., Lin, C. J. and Lin, C. T., "A Functional-Link-Based Neuro-Fuzzy Network for Nonlinear System Control," *IEEE Trans. Fuzzy Syst.*, **16**(5), 1362-1378, 2008.

[2] Chen, C. S., "TSK-Type Self-Organizing Recurrent-Neural-Fuzzy Control of Linear Microstepping Motor Drives," *IEEE Trans. Power Electr.*, **25**(9), 2253-2265, 2010.

[3] Chen, C. S. and Chen, H. H., "Robust Adaptive Neural-Fuzzy-Network Control for the Synchronization of Uncertain Chaotic Systems," *Nonlinear Analysis: Real World Appl.*, **10**(3), 1466-1479, 2009.

[4] Chen, H. K., "Chaos and Chaos Synchronization of A Symmetric Gyro with Linear-Plus-Cubic Damping," *Journal of Sound Vibration*, **255**(4), 719-740, 2002.

[5] Chen, Y. Q., Wang, J., Chan, W. L. and Tsang, K. M., "Chaos Synchronization of Coupled Neurons under Electrical Stimulation via Robust Adaptive Fuzzy Control," *Nonlinear Dynamics*, **61**(4), 847-857, 2010.

[6] Cheng, K. H., Hsu, C. F., Lin, C. M., Lee, T. T. and Li, C., "Fuzzy-Neural Sliding-Mode Control for DC-DC Converters Using Asymmetric Gaussian Membership Functions," *IEEE Trans. Ind. Electron.*, **54**(3), 1528-1536, 2007.

[7] Golea, N., Golea, A. and Benmahammed, K., "Fuzzy Model Reference Adaptive Control," *IEEE Trans. Fuzzy Syst.*, **10**(4), 436-444, 2002.

[8] Hsu, C. F., "Self-Organizing Adaptive Fuzzy Neural Control for a Class of Nonlinear Systems," *IEEE Trans. Neural Netw.*, **18**(4), 1232-1241, 2007.

[9] Hsu, C. F., Chung, C. M., Lin, C. M. and Hsu, C. Y., "Adaptive CMAC Neural Control of Chaotic Systems with a PI-Type Learning Algorithm," *Expert Systems with Appl.*, **36**(9), 11836-11843, 2009.

[10] Juang, C. F., "A TSK-Type Recurrent Fuzzy Network for Dynamic Systems Processing By Neural Network and Genetic Algorithms," *IEEE Trans. Fuzzy Syst.*, **10**(2), 155-170, 2002.

[11] Juang, C. F. and Lo, C., "Zero-Order TSK-Type Fuzzy System Learning Using a Two-Phase Swarm Intelligence," *Fuzzy Sets Syst.*, **159**(21), 2910-2926, 2008.

[12] Lin, C. J., "An Efficient Immune-Based Symbiotic Particle Swarm Optimization Learning Algorithm for TSK-Type Neuro-Fuzzy Networks Design," *Fuzzy Sets Syst.*, **159**(21), 2890-2909, 2008.

[13] Lin, C. M. and Hsu, C. F., "Neural Network Hybrid Control for Antilock Braking Systems," *IEEE Trans. Neural Netw.*, **14**(2), 351-359, 2003.

[14] Lin, C. M. and Hsu, C. F., "Supervisory Recurrent Fuzzy Neural Network Control of Wing Rock for Slender Delta Wings," *IEEE Trans. Fuzzy Systems*, **12**(5), 733-742, 2004.

[15] Lin, C. M., Lin, M. H. and Peng, Y. F., "Synchronization of Chaotic Gyro Systems Using Recurrent Wavelet CMAC," *Cybern. and Syst.*, **41**(5), 391-405, 2010.

[16] Lin, C. T. and Lee, C. S. G., Neural Fuzzy Systems: A Neural-Fuzzy Synergism to Intelligent Systems, Upper Saddle River, NJ: Prentice-Hall, 1996.

[17] Lin, F. J., Shieh, H. J., Shieh, P. H., and Shen, P. H., "An Adaptive Recurrent-Neural-Network Motion Controller for X-Y Table in CNC Machine," *IEEE Trans. Systems Man Cybern. Part B*, **36**(2), 286-299, 2006.

[18] Miguel, H. and Yu, T., "Adaptive Output-Feedback Decentralized Control of a Class of Second Order Nonlinear Systems Using Recurrent Fuzzy Neural Networks," *Neurocomputing*, **73**(1), 461-467, 2009.

[19] Nauck, D., Klawonn, F. and Kruse, R., Foundations of Neuro-Fuzzy Systems, New York: Wiley, 1997.

[20] Shahnazi, R. and Akbarzadeh-T, M., "PI Adaptive Fuzzy Control with Large and Fast Disturbance Rejection for a Class of Uncertain Nonlinear Systems," *IEEE Trans. Fuzzy Syst.*, **16**(1), 187-197, 2008.

[21] Slotine, J. J. E. and Li, W. P., *Applied Nonlinear Control*, Englewood Cliffs, NJ: Prentice-Hall, 1991.

[22] Tseng, C. S., "A Novel Approach to H_∞ Decentralized Fuzzy-Observer-Based Fuzzy Control Design for Nonlinear Interconnected Systems," *IEEE Trans. Fuzzy Syst.*, **16**(5), 1337-1350, 2008.

[23] Velayutham, C. S. and Kumar, S., "Asymmetric Subsethood-Product Fuzzy Neural Inference System (ASuPFuNIS)," *IEEE Trans. Neural Netw.*, **16**(1), 160-174, 2005.

[24] Wang, J., Deng, B. and Tsang, K. M., "Chaotic Synchronization of Neurons Coupled with Gap Junction under External Electrical Stimulation," *Chaos Solitons and Fractals*, **22**(2), 469-476, 2004.

[25] Wang, Q. Y., Lu, Q. S., Chen, G. R., Guo, D. H., "Chaos Synchronization of Coupled Neurons with Gap Junctions," *Phys. Lett. A*, **356**(1), 17-25, 2006.

[26] Wai, R. J. and Chen, P. C., "Intelligent Tracking Control for Robot Manipulator Including Actuator Dynamics via TSK-Type Fuzzy Neural Network," *IEEE Trans. Fuzzy Syst.*, **12**(4), 552-560, 2004.

[27] Yang, Y. S. and Zhou, C. G., "Adaptive Fuzzy H_∞ Stabilization for Strict-Feedback Canonical Nonlinear Systems via Backstepping and Small-Gain Approach," *IEEE Trans. Fuzzy Syst.*, **13**(1), 104-114, 2005.

[28] Zhang, T., Wang, J., Fei, X. Y., and Deng, B., "Synchronization of Ccoupled FitzHugh-Nagumo Systems via MIMO Feedback Linearization Control, *Chaos Solitons and Fractals*, **33**(1), 194-202, 2007.